Available online at www.sciencedirect.com

SciVerse ScienceDirect

Procedia Technology 4 (2012) 9 – 18

Procedia Technology

C3IT-2012

Performance Analysis of a Ge-on-Si Resonant Cavity Enhaced Schottky Photodetetor for Optical Communication at 1.55 μm

H.S.Dutta[a], N.R.Das[b]

[a]*Kalyani Government Engineering College, Kalyani,PIN-741235,India.*
e-mail*: himadri.dutta@gmail.com*
[b] *Instite of Radio Physics & Electronics,University of Calcutta,Kolkata,PIN-700009,India.*

Abstract

In this paper, performance of a Ge-on-Si Resonant-Cavity-Enhanced (RCE) Schottky Photodetector at 1.55□m has been investigated considering the effects of carrier confinements at the Si/Ge heterointerface. The transit-time delay and loss of carriers by recombination have been included in the model to calculate photocurrent, bandwidth, quantum efficiency and bandwidth-quantum efficiency product of the photodiode. Results show that the effect of carrier confinements plays a significant role on the bandwidth as well as quantum efficiency of the photodetector at low-bias. Possible optimum designs of the photodetector at different biases have been suggested in the paper. Noise equivalent bandwidth, dark current, and minimum detectable power are shown for different dimensions of the photodiode and biases indicating the role of heterointerface confinement of carriers.

Keywords: Frequency response; 3-dB bandwidth; quantum efficiency; Resonant cavity enhanced schottky photodetector; noise equivalent bandwidth; dark current; minimum detectable power;

1. Introduction

In recent years, optical fiber communication has played a significant role in the rapid evolution of Information Technology. The ever-increasing and widespread use of data communications has stimulated the development of optoelectronic technologies for reliable photonic components and subsystems with adequate efficiencies and speed of response [1]. Because of the inherent high speed and high density data transfer capabilities of an optical communication system, many efforts have been devoted to move from electrical to optical system. High-speed low-noise photodetectors are the demands in several applications including local area networks, chip-to-chip interconnects, fiber-to-the-home communications, etc. [2]. Commonly used wavelengths for long-distance data transmission are 1.3 μm and 1.55 μm, corresponding to the minimum dispersion and minimum attenuation respectively of silica optical fiber. Researchers all

2212-0173 © 2012 Published by Elsevier Ltd.
doi:10.1016/j.protcy.2012.05.002

over the world are putting tremendous effort to build suitable optoelectronic integrated circuits (OEIC) working in wavelength range 1.3 - 1.55 μm [2-4]. The choice of material is critical for the design of photonic devices when large numbers of devices are integrated on a single chip. The detectors commonly used for long-haul communication systems are based on III-V semiconductor materials [5, 6]. Though III-V compound semiconductors and their alloys show superior performance, the main disadvantage of the material system is high cost, particularly for short-distance communication links. In this respect, Si based photodetectors seem attractive due to the following reasons. The cost of the material is low and Si is one of the natural elementary resources with the large quantity on earth. Besides, the insulators of Si, such as SiO_2 and Si_3N_4, have far better properties than other semiconductor insulators, and the processes to fabricate Si-based insulators are well-established than other insulators. Si has more than three times higher thermal conductivity than GaAs, which reduces the requirement of external cooling. This is important when large numbers of devices are integrated on a single chip and the clock frequency is increased, which raises the power consumption [7].

There are some fundamental problems in using Si as a photodetector material. The cut-off wavelength of Si being ~ 1.1μm, Si photodetectors are not suitable for operation around the long-haul wavelengths of 1.3 and 1.55 μm. Further, being an indirect band gap material Si exhibits poor absorption coefficient. The problems of very low absorption and low cut-off wavelength may be overcome by using lower bandgap Ge, another group IV semiconductor material [2, 8, 9]. Though Ge is also an indirect bandgap (E_g = 0.66 eV) material like Si, its direct bandgap (E_g = 0.8 eV) is only 140 meV above the dominant indirect bandgap. So, Ge offers much higher optical absorption in 1.3–1.55μm wavelength range, thus making Ge-based photodetectors promising candidates for Si photonics integration. However, the 4% lattice mismatch between Ge and Si places challenging obstacle towards monolithic integration of high-quality low dislocation density Ge devices through Ge on Si heteroepitaxy. Recently, a two step ultra-high vacuum / CVD process followed by cyclic thermal annealing has been developed, by which a high quality Ge epilayer on Si has been grown with substantially reduced threading dislocation density within the Ge film [10, 11]. Technological achievements in growth of high quality Ge films on Si wafers have opened up the possibility of low cost Ge-based photodetectors for near infrared communication bands and high resolution spectral imaging with high quantum efficiencies. Thus, Ge has emerged out as a promising material for the active layer of a photodetector. In this paper, the performance of Ge-based resonant cavity enhanced Schottky photodetectors for optical communication is investigated. Schottky photodetectors are very attractive for their relatively simple fabrication process, which enables easy integration with discrete devices and integrated circuits [12]. A thin active layer gives large bandwidth (transit-time limited) of the photodetector, while a thick layer is preferred for high quantum efficiency. To increase the sensitivity of the detector, quantum efficiency should be increased without sacrificing bandwidth. This can be achieved by encapsulating the photodetector in a resonant cavity [2, 13, 14]. The sensitivity of a photodetector is largely controlled by noise. Thermal noise and shot noise are the two major contributors to the noise performance of the photodetector [15, 16]. It may be noted here that because of the band discontinuity at the Si/Ge interface, carriers get trapped (confined) there and, hence, it may affect the noise arising out of the transit of carriers in the device.

The following sections of this paper are organized as follows. The photodetector (PD) structure considered for analysis of noise performance is mentioned in section 2. In section 3, analyses for photocurrent in the photodetector are given. The noise currents and minimum detectable optical power of the photodetector is calculated in section 4. The results and discussions are given in section 5. Finally, in section 6, a conclusion is given.

2. The Device Structure

Schematic layer structure of a back-illuminated Ge-on-Si RCE Schottky photodetector is shown in Fig. 1. Here, a lightly doped intrinsic (i) semiconductor layer of Ge (active layer) has been embedded between the metal layer and p^+ semiconductor (Si) layer. Schottky contact is formed between the top *Au* contact and the Ge film. At the junction of the metal and *i*-layer a depletion layer is formed, the width of which depends both on the concentration of the fixed charges within the *i*-layer and the reverse bias voltage. Si/SiO_2 combination serves as the bottom mirror, and the Au metal layer serves as the top mirror of the resonant cavity [10, 13]. To reduce reflection losses, SiO_2 antireflection coating is used at the bottom on the side of illumination. The absorption layer is made of low bandgap material (Ge) while the *p* layer is made of high bandgap material (Si). Light of wavelength λ is assumed to be incident on the p^+ side which acts as a window layer, and the absorption takes place in the *i* (Ge) layer, which is the active layer of the photodetector. In this calculation, it is assumed that the intrinsic layer is undoped. In an actual case, however, it is found that this layer is unintentionally doped with *n* or *p* type impurity depending on fabrication steps, but this doping concentration is assumed to be negligibly small in this work.

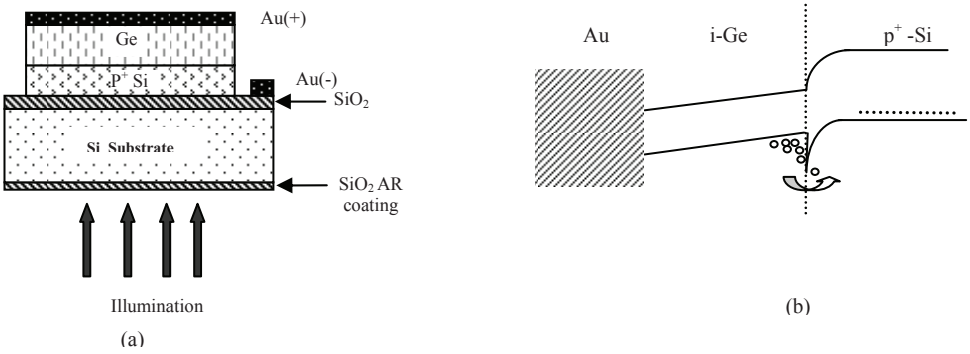

Fig.1 RCE Ge-on-Si schottky photodiode (PD): (a) Schematic cross-section, (b) Energy-band diagram showing hole-confinement at P-Si/Ge heterointerface .

3. Photocurrent Calculation

To calculate the photocurrent, we solve the carrier continuity equations along with appropriate boundary conditions. For example, the continuity equation for holes, assuming constant field, may be written as

$$\frac{\partial p(x,t)}{\partial t} + v_h \frac{\partial p(x,t)}{\partial x} = g(x,t) - \frac{(p - p_0)}{\tau_h} \qquad \ldots(1)$$

where v_h is the velocity of holes, τ_h is recombination time for holes, and $g(x,t)$ is the generation rate of electron-hole pairs given by

$$g(x,t) = \frac{P_{inc}\alpha(1-R_f)e^{-\alpha d}[e^{\alpha\{L-x\}} + R_b e^{-\alpha\{L-x\}}]}{Ahv\left[1-2\sqrt{R_1 R_2}e^{-\alpha d}\cos(2\beta L + \varphi_1 + \varphi_2) + R_f R_b e^{-2\alpha d}\right]}\delta(t), \qquad \ldots(2)$$

where P_{inc} is the incident optical power, h is the Planck's constant, ν is the optical frequency, α is the absorption coefficient of Ge, $R_f(R_b)$ and $\varphi_1(\varphi_2)$ are the reflectivity and phase shift respectively due to penetration of light at the front(back) mirror, $\delta(t)$ is the unit impulse (light) function of time, A (d) is the active area (thickness) of the photodetector, L is the length of the cavity, and β is the propagation constant. In the present analysis / computation, the length of the cavity (L) is so assumed that the condition $2\beta L + \varphi_1 + \varphi_2 = 2m\pi$ is satisfied.

At the hetero-interface between P-Si and i-Ge, band-offsets occur in the valence band and holes are confined as shown in the energy band diagram [Fig. 1(b)]. To include the effect of this confinement in the photocurrent calculation, we assume that the holes from this potential trap are emitted by slow thermionic

emission over the potential barrier. So, it takes a long time for holes to reach the metal contacts and some of the holes are lost due to the recombination during confinement at the hetero-interface. To consider the effect of this hole confinement, rate equation is to be solved [17, 18]. Knowing the position (x) dependent electron and hole densities in the frequency domain, denoted by $N(\omega,x)$ and $P(\omega,x)$ respectively, the average current density in the photodetector is calculated using relation

$$J(\omega) = \frac{q}{d}\int_0^d [N(\omega,x)v_e + P(\omega,x)v_h]dx \cdot \qquad \ldots(3)$$

Final expression for the current including the parasitic RC effect is given by [17]

$$I_p(\omega) = \frac{qP_{inc}}{h\nu\, d(1+j\omega RC)}\left[\frac{v_h e_{ho}}{e_{ho}+1/\tau_h+j\omega}\left\{(R_b - R_f\exp[-\alpha d])\left(\frac{1-\exp[-j\omega d/v_h]}{j\omega}\right)\right.\right.$$
$$\left. + \frac{R_f}{\alpha v_h + j\omega}(1-\exp[-\alpha d - j\omega d/v_h]) + \frac{R_b}{\alpha v_h - j\omega}\cdot(\exp[-\alpha d]-\exp[-j\omega d/v_h])\right\} + \qquad \ldots(4)$$
$$v_e\left(R_f - R_b\exp[-\alpha d]\right)\left(\frac{1-\exp[-j\omega d/v_e]}{j\omega}\right) + \frac{v_e R_b}{\alpha v_e + j\omega}(1-\exp[-\alpha d - j\omega d/v_e]) +$$
$$\left.\frac{v_e R_f}{\alpha v_e - j\omega}\cdot(\exp[-\alpha d]-\exp[-j\omega d/v_e])\right]$$

where v_e is the velocity of electrons and e_{ho} is the rate of thermionic emission of holes from the interface trap in the valance band calculated using the relation

$$e_{ho} = K\exp(-qe_{vd}/k_B T), \qquad \ldots(5)$$

where e_{vd} is the effective barrier for holes in the valence band interface and K is a constant [18].
The quantum efficiency is calculated using the relation

$$\eta = I_p(0)h\nu / qP_{inc}, \qquad \ldots(6)$$

Where, $I_p(0)$ is the dc photocurrent obtained putting ω=0 in Eq.(4). This quantum efficiency is also affected by the carrier confinement at the heterointerface.

4. Calculation of Noise currents

In this section, the mean square noise currents due to thermal noise ($\langle i_T^2 \rangle$) and shot noise ($\langle i_S^2 \rangle$) are calculated for the Ge-based schottky photodetector. The total r.m.s. noise current is then obtained using the relation

$$\sqrt{\langle i_N^2 \rangle} = \sqrt{\langle i_T^2 \rangle + \langle i_S^2 \rangle} \qquad \ldots(7)$$

4.1. Thermal Noise

Thermal noise (or Johnson noise) has its origin in the thermal agitation of the electrons inside an electrical conductor at equilibrium, which happens regardless of any applied voltage. Thermal noise is approximately Gaussian in nature (white noise) and is independent of signal current. The mean square thermal noise current can be expressed as [1]

$$\langle i_T^2 \rangle = \frac{4k_B TB}{R_{eq}} \qquad \ldots(8)$$

where k_B is the Boltzmann constant, T is temperature (K), B is noise equivalent bandwidth and R_{eq} is the equivalent resistance seen from the output ,

$$R_{eq} = [1/(R_D + R_s) + 1/R_L]^{-1}, \qquad \ldots(9)$$

where R_D (R_S) is the shunt (series) resistance of the photodiode and R_L is the load resistance. The noise equivalent bandwidth (B) is given by

$$B = \frac{1}{I_p^2}\int_0^\infty \left|I_p(\omega)\right|^2 d\omega \,, \qquad \ldots (10)$$

where $I_p(\omega)$ is the photocurrent at frequency ω. The calculation of photocurrent is mentioned in the next subsection.

4.2. Shot Noise

Shot noise arises due to the randomness in the generation of current in the device. The shot noise due to the statistical nature of the production and collection of photoelectrons in a photodetector is known as quantum noise. Besides photocurrent, there is current due to the thermally generated carriers in the reverse biased diode in the absence of light. This dark current (I_D) also contributes to the shot noise in a photodetector. The mean square shot noise current is then given by

$$\left\langle i_S^2 \right\rangle = 2q(I_p + I_D)B \,, \qquad \ldots(11)$$

where q is the electronic charge.

4.3. Dark Current

To calculate the dark current we have considered contributions from diffusion current and generation-recombination current [20] due to thermally generated carriers within the device. The diffusion current due to these thermally generated minority carriers in the absence of light can be derived as

$$I_{D\_diff} = qn_i^2 A\left(\frac{\sqrt{D_n/\tau_n}}{N_A} + \frac{e_{ho}\tau_h}{e_{ho}\tau_h + 1}\frac{\sqrt{D_p/\tau_h}}{N_D}\right)\left[1 - \exp\left(-\frac{qV}{k_B T}\right)\right] \qquad \ldots(12)$$

where n_i is the intrinsic carrier concentration, N_A (N_D) is the doping density in the p (n) region, τ_n is the recombination time of electrons and V is the applied reverse bias. In Schottky diodes, there is thermal emission of electrons from the metal to the semiconductor across the Schottky barriers to contribute to the diffusion current of electrons [2]. As the photodiode is operated under the reverse bias, this emission current is negligible. In general, the contribution from the diffusion current has significance particularly for the undepleted regions or when the field is very low. In the depleted region with high field, the dark current is mainly dominated by the generation-recombination current due to thermally generated carriers. The generated holes during transit get confined at the heterointerface due to potential barrier arising from the valence band discontinuity. Its contribution to the total current is affected due to their recombination during the confinement. The dark current due to generation-recombination of these thermal electron-hole pairs in the depletion region is given by

$$I_{D\_gr} = \frac{qn_i d}{4}\left[\frac{1}{\tau_n} + \frac{e_{ho}}{e_{ho}\tau_h + 1}\right]\left[1 - \exp\left(-\frac{qV}{k_B T}\right)\right]. \qquad \ldots(13)$$

The total dark current is the sum of these two currents.

4.4. Minimum Detectable Power

The weakest signal that can be detected by a photodetector in the presence of noise is usually given by the noise equivalent power of the system which corresponds to unit signal-to-noise ratio. This is also defined as the minimum detectable optical power in the presence of noise. With this definition, the minimum detectable power (P_{min}) is given by

$$P_{\min} = \frac{2h\nu}{\eta q}\sqrt{\left(q(I_p + I_D) + \frac{k_B T}{R_{eq}}\right)B} \qquad \ldots(14)$$

5. Results and Discussion

In Fig.2(a), the quantum efficiency has been plotted as a function of wavelength to verify our model with the experimental data (at zero bias) given in [10] and reasonably good agreement has been found. Simulated data taken from [10] are also plotted in this figure. It has been seen from the figure that the experimental data show closer agreement with our model than with the simulated data of [10]. Present model considers the effect of carrier confinement, which has possibly not been considered in the simulation given in [10] resulting in overestimation of the responsivity at zero bias. Throughout the study, the cavity parameters are chosen in such a way that the quantum efficiency always becomes maximum due to resonance in the cavity.

In Fig. 2(b), the quantum efficiency at 1.55μm wavelength has been plotted as a function of active layer thickness (*d*) for different bias voltages using Eq. (4, 5 and 6). It can be seen from the figure that the quantum efficiency initially increases with increase in *d*, and then decreases after attaining peak. The particular value of *d* for which peak occurs depends on the applied bias. This is due to the fact that with increase in layer thickness, quantum efficiency increases mainly for enhanced absorption. However, some of the thermionically emitted holes are lost by recombination. Thus, overall number of holes, collected at the contacts and, hence, quantum efficiency reduces due to the carrier confinement effect. But, due to the usual predominant effect of *d* on quantum efficiency, quantum efficiency increases with increase in *d*. The usual variation of quantum efficiency with *d* is that it starts to saturate as *d* increases. So, the decrease of the quantum efficiency at higher value of *d* is due to the predominant effect of the carrier confinement. The effect of confinement is again bias dependent. As the applied bias increases, the carrier confinement effect starts to dominate for larger *d* and so, the peak position shifts towards right with increase in bias.

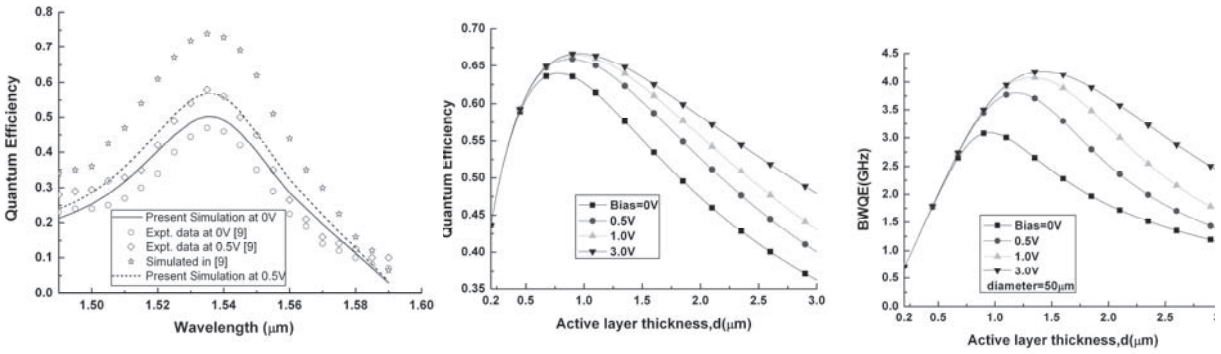

Fig. 2(a) Plot of quantum efficiency as a function of wavelength, λ for the reverse bias of 0V for model verification. Experimental data are taken from [9]. (b)Plot of resonant quantum efficiency as a function of d for different bias. (c)Plot of bandwidth quantum efficiency product (BWQE) as a function of active layer thickness d for different bias keeping diameter is fixed at 50μm.

Bandwidth-quantum efficiency product is plotted as a function of active layer thickness as shown in Fig. 2(c) keeping diameter constant at 50μm. In this figure, the study has been shown for a particular diameter but for different biases. The shifts in peak position increases with increase in bias and will ultimately remain unaltered because of the vanishing effect of carrier confinement at hetero-interface at large bias. The product initially increases and then decreases after attaining maxima with increase in *d*. For higher diameter the peaks are shifted to higher values of *d*.

Using Eq. (4, 5 and 6), quantum efficiency of a Ge-on-Si RCE Schottky photodetector is plotted as a function of R_f for different values of R_b keeping thickness of the active layer (*d*) constant. Figs. 3(a) and (b) are shown for $d = 0.2\mu m$, and $0.8\mu m$ respectively. It can be seen in Fig. 3(a) that quantum efficiency (QE) initially increases with R_f, reaches a maximum value and, then, decreases, showing an optimum R_f

(called R_{f_opt}) for which QE reaches maximum. If reflectivity is very small then a large portion of light goes out of the cavity. On the other hand, if the reflectivity is very high, then only a very small amount of light enters the cavity containing the photodetector. Thus, for certain values of reflectivity, quantum efficiency becomes maximum. It may be also seen that the maximum point shifts to the right with increase in R_b. This can be explained as follows. For high R_b, R_f should also be increased to get maximum quantum efficiency, because, otherwise the significant fraction of light would go outside of the cavity through front mirror. So, R_{f_opt} increases with increase of R_b. Similar nature of variations shown in the Fig. 3(b) also. But, it may be noted that the maxima occurs at lower values of R_f, (and R_b) with increase in active layer thickness. This occurs because the large thickness causes increased absorption and, so, the leakage of light out of the cavity is small even if R_f reflectivity is small. So, maximum value of QE occurs at small R_f, (and R_b) as d is increased and variation of QE with R_f, occurs slowly around the maxima. The optimum thickness for quantum efficiency at different biases and the maximum values of QE are summarized in Table 1.

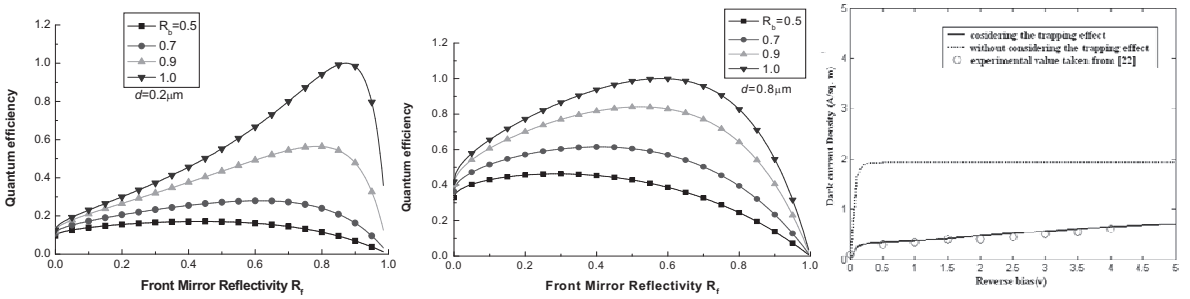

Fig. 3(a) Plot of quantum efficiency at 1.55μm as a function of front mirror reflectivity R_f for different back mirror reflectivity R_b, at active layer thickness d= 0.2 μm, (b) Plot of quantum efficiency at 1.55μm as a function of front mirror reflectivity R_f for different back mirror reflectivity R_b, at active layer thickness d= 0.8 μm, (c) Plot of dark current as a function of reverse bias. The symbols correspond to data extracted from the experimental results given in [12] and dotted line for dark current without considering carrier confinement effect.

In this paper maxima of bandwidth-quantum efficiency product are studied to find some optimum designs. The design values which satisfy the minimum bandwidth or quantum efficiency requirements in an application can be chosen from the optimum design data. Some optimum values of d for which the bandwidth-quantum efficiency product attain maxima are indicated in Table 2. As described earlier, there exist optimum values of d which gives maximum bandwidth-quantum efficiency product at different diameters and biases. It is seen in Table 2 that this optimum active layer thickness increases with bias,

R_b	d=0.2 μm		d=0.5 μm		d=1.1 μm	
	R_{f_opt}	QE_{max}	R_{f_opt}	QE_{max}	R_{f_opt}	QE_{max}
0.5	0.44	0.17	0.36	0.35	0.24	0.55
0.6	0.53	0.22	0.43	0.41	0.29	0.62
0.7	0.61	0.28	0.50	0.50	0.33	0.69
0.8	0.70	0.38	0.57	0.61	0.38	0.78
0.9	0.79	0.56	0.64	0.77	0.43	0.88
1.0	0.88	1.00	0.71	1.00	0.48	1.00

Table 1. Some optimum values of front mirror reflectivity R_{f_opt} for maximum quantum efficiency (QE_{max}) for λ=1.55μm

Bias (V)	Diameter=25 μm		Diameter=50 μm		Diameter=100 μm	
	d'_{opt} (μm)	BW-QE_{max} (GHz)	d'_{opt} (μm)	BW-QE_{max} (GHz)	d'_{opt} (μm)	BW-QE_{max} (GHz)
0	0.63	7.67	0.95	3.09	1.55	1.09
0.25	0.73	8.35	1.07	3.52	1.65	1.23
0.5	0.77	8.62	1.17	3.81	1.73	1.34
0.75	0.80	8.71	1.27	3.98	1.87	1.42
1.0	0.80	8.74	1.33	4.08	2.00	1.49
1.5	0.80	8.75	1.37	4.16	2.10	1.57
2.0	0.80	8.75	1.40	4.18	2.25	1.61
3.0	0.80	8.75	1.40	4.19	2.35	1.64

Table 2. Some optimum values of d (say, d'_{opt}) for maximum bandwidth – quantum efficiency product ($BWQE_{max}$)

ultimately attaining a constant value at higher biases. The variation of optimum *d* with diameter of the detector is also shown there. As the diameter increases for a particular bias, the value of optimum *d* for the maximum bandwidth-quantum efficiency product increases significantly. But, the maximum value of the product decreases with the increase of active area diameter. The optimization table is very useful for the design and fabrication of the photodetector, to achieve the maximum bandwidth-quantum efficiency product by selecting the parameters properly.

The dark current is computed by Eq. (12 and 13) to verify the model for dark current, a plot is shown in Fig. 3(c), as a function of bias. The experimental data for comparison are taken from literature [19] where the device is a Ge *p-i-n* photodetector with Ge as the intrinsic layer and Si as *p* and *n* layer. So the confinement effect for electrons has also been considered in this computation. However, the potential barrier for electrons being less than that of holes, the confinement effect of electrons is small. It is clear from the figure that the model results fit well with the experimental data. The dark current in the absence of the confinement effect is shown by the dotted line.

The photocurrent and dark current with respect to reverse bias voltage are plotted in Fig. 4(a) for an input power of 100μW. In all the results, the reflectivity of the top (bottom) mirror of the resonant cavity has been assumed to be 80% (55%). The dark current is less than the photocurrent mainly because of the operation of the photodiode under reverse bias. Photocurrent can be increased by increasing the input optical power. When the bias voltage is very small the dark current is nearly zero and it increases with voltage to finally reach the saturation value. It has been seen that the main contribution to the dark current comes from the generation-recombination (thermal) current. The dotted line shows the current in the absence of carrier confinement. The effect of carrier confinement is significant near the knee of the curves. The graph shows that both photocurrent and dark currents are reduced due to confinement effect.

Both bandwidth and noise equivalent bandwidth (NEB) are nearly similar in nature with a little exception because of the way they are defined. While a peak in bandwidth is desired, the same in noise equivalent bandwidth is not desired. So, the noise equivalent bandwidth to bandwidth ratio may give some important information for noise performance with reference to high frequency performance. In Fig. 4(b), the ratio of noise equivalent bandwidth to photodetector bandwidth has been plotted as a function of active layer thickness for different diameters of the active area for no bias. We see that the ratio is high for low *d*, and then decreases with increase in *d*. In some cases, the ratio may show a minimum, which means that there is an optimum choice for *d*, where noise performance can be improved without affecting its high frequency performance.

The variation of P_{min} with thickness is shown in Fig. 4(c) at 0V. With the increase of *d*, P_{min} increases, the increment being more rapid for smaller thicknesses where the noise equivalent bandwidth is

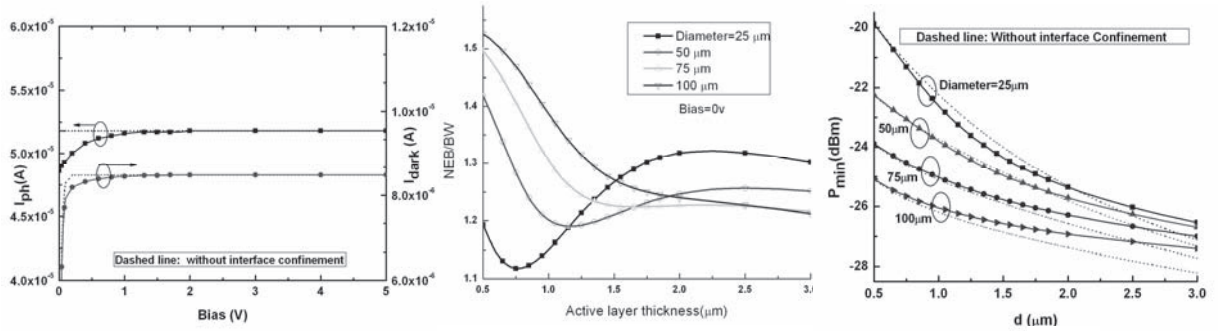

Fig. 4(a) Plot of photocurrent and dark current as a function of reverse bias, (b) Plot of noise equivalent bandwidth and bandwidth ratio as a function of active layer thickness, d for different values of detector diameter at No Bias, (c) Plot of Minimum detectable power as a function of active layer thickness for different active area diameter at no bias.

dominated by RC-effect. At larger *d*, the noise equivalent bandwidth is transit-time limited and so the effect of confinement also becomes relatively significant. It may be seen that the effect of confinement is to deteriorate the P_{min} except for a smaller diameter (e.g. 25μm) and a smaller thickness (around 1μm) when the confinement improves the minimum detectable power. At low bias, the shot noise due to photocurrent is low, so the minimum detectable signal power (optical) is low. The effect of confinement is also shown by dotted lines.

6. Conclusion

In the present study, we have investigated the bandwidth, quantum efficiency, their product, and noise currents in a Ge-on-Si RCE Schottky photodetector considering the carrier confinement effect at the Si/Ge hetero-interface. The model results are verified with experimental data taken from literature. It has been seen that, the quantum efficiency becomes a function of applied bias and thickness because of the carrier confinement effect. Bandwidth-quantum efficiency product attains a peak, which moves towards higher thicknesses as the applied bias increases. Some possible optimum values of *d* for maximum bandwidth and also for maximum bandwidth-quantum efficiency product are given in tabular form. It has been seen that the noise equivalent bandwidth of the detector is low at low bias because of the recombination of holes during confinement at the Si/Ge hetero-interface. For high enough bias, the confinement is absent and the NEB reaches a constant value determined by the transit time due to the saturation velocity of carriers and the RC effect. The NEB/BW ratio indicates there may exist choice of thickness for which noise performance can be improved without affecting its high frequency performance. In the noise current it has been seen that the thermal noise and the shot noise due to photocurrents are mainly significant in the noise performance of the photodetector. Depending on the bias and dimensions, the heterointerface confinement of holes affect the minimum detectable power. With small diameter and small thickness of the PD and operating at low bias, the noise performance can be improved.

References

1. G. Keiser, “Optical Fiber Communications”, *McGraw-Hill Int., Singapore,* 1989
2. P. Bhattacharya, “Semiconductor Optoelectronic Devices”, Second Edition, *New Delhi: Prentice-Hall India,* 2004.
3. O. I. Dosunmu, D. D. Cannon, M. K. Emsley, B. Ghyselen, J. Liu, L. C. Kimerling, and M. S. Ünlü, “Resonant Cavity Enhanced Ge Photodetectors for 1550 nm Operation on Reflecting Si Substrates”, *IEEE J. Sel. Topics. in Quant. Electro*., vol. 10, p. 694, 2004.
4. C. Li, C. J. Huang, B. Cheng, Y. Zuo, L. Luo, J. Yu and Q. Wang, “SiGe/Si Resonant-Cavity-Enhanced Photodetectors for 1.3μm Operation Fabricated Using Wafer Bonding Techniques”, *J. Appl. Phys.,* vol. 92, p. 1718, 2002.
5. W. A. Wohlmuth, J. -W. Seo, P. Fay, C. Caneau, and I. Adesida, “A High-Speed ITO–InAlAs–InGaAs Schottky-Barrier Photodetector”, *IEEE Photon. Technol. Lett.,* vol. 9, p. 1388, 1997.[5]
6. M. S. Ünlü, K. Kishino, J. I. Chyi, J. Reed, S. N. Mohammad, and H. Morkoc, “Resonant Cavity Enhanced AlGaAs/GaAs Heterojunction Phototransistors with an Intermediate InGaAs Layer in the Collector”, *Appl. Phys. Lett.*, vol. 57, p. 750, 1990.
7. L. C. Kimerling, “Silicon Microphotonics”, *Appl. Surf. Sc.,* vol. 8, p. 159, 2000.
8. S. J. Koester, J. D. Schaub, and G. Dehlinger, “Germanium-on-SOI Infrared Detectors for Integrated Photonic Applications”, *IEEE J. Sel. Top Quantum Electron,* vol. 12, p. 1489, 2006.
9. S. Klinger, M. Berroth, M. Kaschel, M. Oehme, and E. Kasper, “Ge-on-Si p-i-n Photodiodes with a 3-dB Bandwidth of 49 GHz”, *IEEE Photon. Techno. Lett.,* vol. 21, p. 920, 2009.
10. O. I. Dosunmu, D. D. Cannon, M. K. Emsley, L. C. Kimerling and M. S. Ünlü , “High–speed Resonant Cavity Enhanced Ge Photodetectors on Reflecting Si Substrates for 1550 nm Operation”, *IEEE Photon Technol. Lett.,* vol. 17, p. 175, 2005.
11. H. C. Luan, D. R. Lim, K. K. Lee, K. M. Chen, J. G. Sandland, K. Wada, and L. C. Kimerling, “High Quality Ge Epilayers on Si with Low Threading Dislocation Densities”, *Appl. Phys. Lett.,* vol. 75, p. 2909, 1999.
12. M. Wilson, and S. R. J. Brueck, “A Simple High-Speed Si Schottky Photodiode”, *IEEE Photon. Technol. Lett.,* vol. 3, p. 360, 1991.
13. M. S. Ünlü, and S. Strite, “Resonant Cavity Enhanced Photonic Devices”, *J. Appl. Phys.*, vol. 78, p. 607, 1995.
14. D. S. Golubović, P. S. Matavulj, and J. B. Radunović, “Resonant Cavity-Enhanced Schottky Photodiode - Modelling and Analysis”, *Semicond. Sci. Technol*., vol. 15, p. 950, 2000.

15. G. N. Milford, C. C. Harb, and E. H. Huntington, "Shot noise limited, microwave bandwidth photodetector design", *Rev. Sc. Instr.*vol. 77, p. 114701, 2006.
16. L. Colace, P. Ferrara, G. Assanto, D. Fulgoni and L. Nash, "Low dark-current germanium-on-insulator near infrared detectors", *IEEE Photon. Technol. Lett.*.vol. 19, p. 1813, 2007.
17. H. S. Dutta, N. R. Das and M. K. Das, "Investigating the Effects of Heterointerface Trapping on the Performance of Ge-Based RCE Schottky Photodiode at 1.55μm", *Sem. Sc. Technol.*, vol. 23,p. 085012, 2008.
18. N. R. Das, and M. J. Deen, "*Calculating the Photocurrent and Transit-Time-Limited Bandwidth of a Heterostructure p-i-n Photodetector*", *IEEE J. Quant. Electron*., vol. 37,p. 1574, 2001.
19. J. Osmond, G. Isella, D. Chrastina, R. Kaufmann, M. Acciarri, and H. V. Kanel, "Ultralow Dark Current Ge/Si(100) Photodiodes with Low Thermal Budget", *Appl. Phys. Lett.*, vol. 94, p. 1, 2009.
20. S. R. Forrest, "Performance of $In_xGa_{1-x}AsyP_{1-y}$ Photodiodes with Dark Current Limited by Diffusion, Generation Recombination and tunneling", *IEEE J. Quant. Electron.*, vol. 17, p, 217, 1981.